

High-temperature structural behaviors of anhydrous wadsleyite and forsterite

DMYTRO M. TROTS,* ALEXANDER KURNOSOV, TIZIANA BOFFA BALLARAN, AND DANIEL J. FROST

Bayerisches Geoinstitut, Universität Bayreuth, D-95440 Bayreuth, Germany

ABSTRACT

The thermal expansion of anhydrous Mg_2SiO_4 wadsleyite and forsterite was comprehensively studied over the temperature ranges 297–1163 and 297–1313 K, respectively, employing X-ray powder diffraction. Experiments were carried out with two separately synthesized samples of wadsleyite (numbered z626 and z627), for which room temperature unit-cell volumes differed by 0.05%, although the determined thermal expansions were identical within error. The high-temperature thermal expansions of wadsleyite and forsterite were parameterized on the basis of the first-order Grüneisen approximation using a Debye function for the internal energy. Values for hypothetical volume at $T = 0$ K, Debye temperature and Grüneisen parameter are 536.86(14) Å³, 980(55) K, 1.28(2) and 537.00(13) Å³, 887(50) K, 1.26(1) for z626 and z627, respectively, with the bulk modulus fixed to a literature determination of 161 GPa. For forsterite, the respective values are 288.80(2) Å³, 771(9) K, and 1.269(2) with a constrained bulk modulus of 125 GPa. These quantities are in good agreement with literature values obtained independently from sound velocity and heat capacity measurements, giving strong support to the applicability of Grüneisen theory in describing the thermal expansion of wadsleyite and forsterite. In addition, high-temperature structural variations were determined for wadsleyite from Rietveld analysis of the X-ray diffraction data. The pronounced anisotropy in thermal expansion of wadsleyite with a more expandable *c*-axis, similar to the compressional anisotropy, arises from specific features of the crystal structure consisting of the pseudolayers of MgO_6 octahedra parallel to the *a*-*b* plane with cross-linking Si_2O_7 dimers along the *c*-axis. Although anisotropic compression and expansion originate from the same structural features, the details of structural changes with pressure differ from those caused by temperature. The longest Mg-O bonds, which are roughly parallel to the *c*-axis in all three octahedral sites of wadsleyite, dominate the compression, but these bonds do not exhibit the largest expansivities.

Keywords: Forsterite, wadsleyite, thermal expansion, Mg_2SiO_4 polymorphs, powder diffraction

INTRODUCTION

The Mg_2SiO_4 polymorphs, forsterite and wadsleyite, are major mineral components within the Earth's upper mantle and transition zone. The olivine-wadsleyite transition of $(\text{Mg,Fe})_2\text{SiO}_4$ is considered to cause a seismically detectable discontinuity in elastic properties at approximately 410 km depth (e.g., Ringwood 1975). Precise information on the physical properties and stability fields of wadsleyite and olivine at high temperatures and pressures is of primary importance to geophysics. To calculate stability fields and seismic wave velocities of mantle minerals, thermodynamic parameters are often refined from high-pressure experimental phase relations and equation of state data. This permits phase boundaries and seismic wave velocities to be determined at conditions beyond the range of experimental measurements and allows multiple studies to be compared and uncertainties in pressure and temperature to be addressed. Such calculations are far more constrained if parameters such as thermal expansivity and bulk modulus can be accurately determined independently. Thermal expansion measurements provide

particularly useful constraints on elastic properties due to very low-experimental uncertainties. However, there is significant divergence between results of previous thermal expansion studies performed on Mg_2SiO_4 polymorphs and a strong divergence in some equations used to parameterize these measurements when extrapolated beyond the measured range.

The thermal expansivity of forsterite has been previously measured up to its melting point of approximately 2150 K by Bouhifd et al. (1996) employing energy-dispersive powder X-ray diffraction. Moreover, Bouhifd et al. (1996) made a comprehensive comparison with results of previous high-temperature diffraction investigations of Skinner (1962), Takeuchi et al. (1984), Vokurka and Rieder (1987), Kajiyoshi (1986), and dilatometry studies of Suzuki et al. (1984), Matsui and Manghnani (1985), and White et al. (1985). Good agreement was observed with the data of Kajiyoshi (1986) and with values optimized by Gillet et al. (1991) and Fei and Saxena (1986) from various high-temperature data. The recent work of Ye et al. (2009) reports expansivity data for anhydrous forsterite up to 889 K obtained using single-crystal X-ray diffraction. Both Bouhifd et al. (1996) and Ye et al. (2009) describe the thermal dependency of the volumetric thermal expansion using linear functions.

* E-mail: d_trots@yahoo.com

Suzuki et al. (1980) measured the thermal expansion of wadsleyite up to 1073 K using X-ray powder diffraction, employing 9 Bragg maxima to derive unit-cell parameters. Grüneisen theory was employed to describe the results and pronounced anisotropy in expansivity of wadsleyite was found, with expansion along the *a*-axis around 1.6 times higher in comparison to the *b*- and *c*-axes [*a*- and *c*-axes in Suzuki et al. (1980) correspond to *c*- and *a*-axes in our crystallographic setting]. *P-V-T* relations of wadsleyite were investigated by synchrotron in situ powder diffraction using a multi-anvil apparatus by Li et al. (2001) and Katsura et al. (2009). The ambient pressure thermal expansion coefficient was, in both cases, described as a linear function of temperature. The studies of Inoue et al. (2004) and Ye et al. (2009) were aimed at clarifying the effects of hydration on the ambient pressure thermal expansion of the Mg₂SiO₄ polymorphs. Both studies made measurements of the room-pressure thermal expansion of anhydrous wadsleyite. The study of Inoue et al. (2004) employed powder X-ray diffraction measurements of 9 diffraction maxima, whereas that of and Ye et al. (2009) used single-crystal X-ray diffraction. Whereas Inoue et al. (2004) described the thermal expansion using a single temperature independent coefficient, Ye et al. (2009) employed a linear temperature dependence.

A comparison between the previous thermal expansion results reveals considerable discrepancies, particularly for wadsleyite, even at room temperature. Although values for $\alpha_{(293\text{ K})}$, for example, of Suzuki et al. (1980), Katsura et al. (2009), Ye et al. (2009), are comparable, they are considerably lower compared to those reported by Li et al. (2001) and Inoue et al. (2004). This fact provoked us to perform high-temperature powder X-ray diffraction experiments on anhydrous wadsleyite and forsterite and to examine a suitable methodology for fitting and extrapolating the data. We compare our results with previous studies and with analyses of previous studies reported in the literature. In addition, temperature-induced structural variations in anhydrous wadsleyite are examined through Rietveld refinement of the synchrotron powder diffraction data.

EXPERIMENTAL AND DATA ANALYSIS

Syntheses

Mg₂SiO₄ forsterite was synthesized from reagent grade MgO and SiO₂. The oxides were dried, ground together in an agate mortar then cold pressed into a pellet and fired at 1673 K for 12 h. The recovered sample was then reground, repressed, and refired three more times before X-ray powder diffraction revealed peaks solely for forsterite (PDF-2/card 34-189).

Approximately 30 mg of wadsleyite was synthesized in a 5000 tonne press at 16 GPa and 1473 K. A powdered sample of forsterite was first dried at 1273 K then placed inside a welded platinum capsule of 2 mm diameter and approximately 3.5 mm long. The capsule was placed inside an 18 mm edge length MgO octahedron pressure medium that contained a cylindrical LaCrO₃ heater. The octahedron was compressed using 54 mm edge length tungsten carbide anvils with 11 mm anvil truncations. Further details are described in Frost et al. (2004). The experimental capsule was compressed then heated to the target temperature for 4 h. The recovered sample was removed from the platinum capsule then crushed and ground.

Fourier transform infrared spectroscopy (FTIR) performed on samples of wadsleyite synthesized at similar conditions has revealed that approximately 150 ppm by weight H₂O can be dissolved in the structure, even if the starting forsterite samples are dried at 1273 K prior to loading (Jacobsen et al. 2005). Using the relationship between the *b/a* ratio and H₂O content of for wadsleyite calibrated by Jacobsen et al. (2005), indicates negligible H₂O concentrations in the two wadsleyite samples (z626 and z627) synthesized for this study.

Powder diffraction

The thermal expansion of forsterite was measured using a furnace mounted on a Philips X'Pert Pro X-ray diffraction system operating in reflection mode, with CoK α_1 ($\lambda = 1.78897 \text{ \AA}$) radiation selected with a focusing monochromator, a symmetrically cut curved Johansson Ge(111) crystal, and a Philips X'celerator detector. The sample was loaded into an Al₂O₃ sample holder with Si+MgO powder added as a standard. The temperature was raised in steps of around 20° to 1313 K. Diffraction patterns were collected from 15–100° in 2 θ . A furnace was calibrated for melting points of indium, aluminum, zinc, silver, and gold. Diffraction patterns were analyzed using the GSAS package (Larson and von Dreele 2004).

Synchrotron powder diffraction

Thermal expansion measurements and in situ structural investigation of the two samples of anhydrous wadsleyite (z626 and z627) were performed at the synchrotron facility HASYLAB/DESY (Hamburg, Germany) with the powder diffractometer at beamline B2 (Knapp et al. 2004a). The samples were ground in an agate mortar and sieved through a mesh. Quartz capillaries 0.3 mm in diameter were filled with powdered wadsleyite and sealed. Subsequently, the capillaries were mounted inside a STOE furnace in Debye-Scherrer geometry, equipped with a Eurotherm temperature control and a capillary spinner. The furnace temperature was measured by a TYPE-N thermocouple and calibrated using the thermal expansion of NaCl (Pathak and Vasavada 1970). A wavelength of 0.68794 Å was selected using a Si(111) double flat-crystal monochromator from the direct white synchrotron beam. The X-ray wavelength was determined from eight reflection positions of LaB₆ reference material (NIST SRM 660a) measured by a scintillation single-counter detector with the analyzer crystal in the front. The diffraction patterns, 19 patterns for z626 and 20 for z627, were collected (15–25 min per pattern in dependence on the synchrotron ring current) at fixed temperatures (2 min for temperature stabilization) during the heating cycles using an image-plate detector (Knapp et al. 2004b) (2 θ range 5–70°). The image plate detector was calibrated using the diffraction pattern of LaB₆, and the wavelength was determined by a scintillation counter/analyzer crystal tandem. An additional pattern was taken at ambient temperature after the heating cycle. All diffraction patterns were analyzed by full-profile Rietveld refinements using the software WinPLOTR (Rodríguez-Carvajal 1993). The peak profile shape was modeled by a pseudo-Voigt function. The background of the diffraction pattern was determined using a linear interpolation between selected data points in non-overlapping regions. The full-profile Rietveld method was applied for the analysis of the synchrotron data. The scale factor, lattice parameters, fractional coordinates of atomic sites and their overall atomic displacement parameter, sample shift, and profile shape parameters were varied during the fitting procedure. The standard absorption correction procedure for cylindrical samples, which is implemented in the “FullProf” package, was applied.

Models for thermal expansion

The thermal expansion of forsterite and wadsleyite was modeled using several different methodologies. The temperature evolution of the volume can be expressed as (Fei 1995)

$$V(T) = V_R \exp \left(\int_{T_R}^T \alpha_{(T)} dT \right) \quad (1)$$

where V_R is the volume at a chosen reference temperature T_R and $\alpha_{(T)}$ is the thermal expansion coefficient. We fitted Equation 1 to experimental V vs. T data (Tables A1–A3¹) at fixed experimental values of V_R and T_R (taken at room temperature, 297 K). A linear expression of the form,

$$\alpha(T) = a_0 + a_1 T \quad (2)$$

was found to give a suitable description of the experimental data. Analysis of the correlation matrix indicates that higher polynomial expressions are unjustified over the temperature range. Such a description of thermal expansion, however, implies non-zero values for expansivity at 0 K and has little underlying theoretical justification for extrapolation to higher temperature. A more physically meaningful

¹ Deposit item AM-12-073, Appendix figures, tables, and materials. Deposit items are available two ways: For a paper copy contact the Business Office of the Mineralogical Society of America (see inside front cover of recent issue) for price information. For an electronic copy visit the MSA web site at <http://www.minsocam.org>, go to the *American Mineralogist* Contents, find the table of contents for the specific volume/issue wanted, and then click on the deposit link there.

parameterization of experimental $V(T)$ dependency can be obtained using first- or second-order Grüneisen approximations for the zero pressure equation of state in which the effects of thermal expansion are considered to be equivalent to elastic strain (Wallace 1998), i.e., for first order:

$$V(T) = \frac{\gamma}{K_0} U(T) + V_0 \quad (3)$$

and for second order:

$$V(T) = \frac{V_0 U(T)}{V_0 K_0 / \gamma - 0.5(K' - 1)U(T)} + V_0 \quad (4)$$

where V_0 is hypothetical volume at $T = 0$, γ is the Grüneisen parameter, assumed to be pressure and temperature independent, K_0 and K' are the isothermal bulk modulus at $T = 0$ K and its first pressure derivate, respectively. The internal energy $U(T)$ can be calculated using the Debye model to describe the energy of the lattice vibrations

$$U(T) = 9Nk_B T \left(\frac{T}{\theta_D} \right)^3 \int_0^{\theta_D/T} \frac{x^3 dx}{e^x - 1} \quad (5)$$

where N is the number of atoms in the unit cell, k_B is Boltzmann constant, and θ_D is Debye temperature. Determinations for K_0 and K' (see Table 1), were taken from the literature while V_0 , γ , and θ_D were allowed to vary during the fitting procedure. Note that, as inferred from Suzuki et al. (1983) and Li et al. (2001), K_0 values for forsterite and wadsleyite at 0 K differ from ambient temperature by <4 GPa. On the other hand, refinements of K_0 in Equations 3 and 4 lead to larger correlations and standard errors for K_0 , estimated to be around 5 GPa. Therefore, the fixing of K_0 to ambient-temperature values will not affect our final results.

While the first-order Grüneisen approximation is generally found to provide a superior fit to low-temperature data, the second-order approximation is generally reported as being more appropriate for the fitting and extrapolation of higher temperature data (Vocadlo et al. 2002; Lindsay-Scott et al. 2007). For reasons of comparison, and to examine the most suitable extrapolation method, both equations were employed in fitting.

The linear expansivities were also described by Equation 1 with unit-cell dimensions a_R , b_R , or c_R at $T_R = 297$ K fixed to experimental values (see Table 2). As with the $V(T)$ description, a linear $\alpha(T)$ expression was found to provide the most suitable fit over the experimental temperature range. Linear expansion can also be described using equations analogous to Equations 3 and 4: (see, as example, Suzuki et al. 1980; Fortes et al. 2007; Senyshyn et al. 2009; Trots et al. 2009) i.e.,

TABLE 1. Volumetric thermal expansion parameters of wadsleyite and forsterite

	Wadsleyite (z626)	Wadsleyite (z627)*	Forsterite
Linear form of thermal expansion with Equations 1 and 2			
a_0 (K ⁻¹)	2.14(7)·10 ⁻⁵	2.34(5)·10 ⁻⁵	3.23(2)·10 ⁻⁵
a_1 (K ⁻²)	1.21(11)·10 ⁻⁸	0.95(9)·10 ⁻⁸	6.3(3)·10 ⁻⁹
R †	0.9995518	0.9997548	0.9999099
First-order Grüneisen approximation, Equations 3 and 5			
K_0 (GPa)	161	161	125
V_0 (Å ³)	536.86(14)	537.00(13)	288.80(2)
θ_D (K)	980(55)	887(50)	771(9)
γ	1.28(2)	1.26(1)	1.269(2)
R	0.9997539	0.9998107	0.9998887
Second-order Grüneisen approximation, Equations 4 and 5			
K_0 ‡	5	5	4
V_0 (Å ³)	536.59(17)	536.70(17)	288.31(4)
θ_D (K)	816(64)	718(57)	483(20)
γ	1.16(2)	1.15(1)	1.139(2)
R	0.9997429	0.9998139	0.9998184

Notes: Values without standard deviations are constrained. A priori values for K_0 and K' for anhydrous wadsleyite and forsterite are taken from references Angel et al. (2001) and Downs et al. (1996), respectively. For reproducing $V(T)$ dependencies according to Equations 1 and 2, use V_0 in Å³. For reproducing $V(T)$ dependencies according to Equations 3–5, use K_0 in Pa, V_0 in m³ and, to obtain a final result in Å³, multiply by a factor of 10³⁰.

*Volumes at 1110 and 1163 K, where forsterite content started to increase, were excluded from the fits.

† The measure of quality of nonlinear regression was determined as $R = 1 - [\sum_i (y_i^{obs} - y_i^{calc})^2] / [\sum_i (y_i^{obs} - \langle y_i^{obs} \rangle)^2]$.

‡ K_0 is same as for first-order Grüneisen approximation.

TABLE 2. Axial thermal expansion parameters of wadsleyite and forsterite

	a_0 (K ⁻¹)	a_1 (K ⁻²)	R
Equations 1 and 2			
Wadsleyite z626			
a (Å)	6.6(3)·10 ⁻⁶	2.8(5)·10 ⁻⁹	0.9987188
b (Å)	5.7(2)·10 ⁻⁶	3.3(4)·10 ⁻⁹	0.9991798
c (Å)	9.1(2)·10 ⁻⁶	5.9(3)·10 ⁻⁹	0.9998351
Wadsleyite z627			
a (Å)	7.3(2)·10 ⁻⁶	2.1(4)·10 ⁻⁹	0.9994481
b (Å)	6.8(1)·10 ⁻⁶	2.1(2)·10 ⁻⁹	0.9997367
c (Å)	9.37(2)·10 ⁻⁶	5.3(3)·10 ⁻⁹	0.9998467
Forsterite			
a (Å)	7.73(6)·10 ⁻⁶	2.27(8)·10 ⁻⁹	0.9998719
b (Å)	12.91(8)·10 ⁻⁶	2.1(1)·10 ⁻⁹	0.999907
c (Å)	11.64(8)·10 ⁻⁶	1.9(6)·10 ⁻⁹	0.9999257

Notes: The fits were performed to the data sets $a(b, c)$ vs. T , where unit-cell dimensions were taken in Å and temperature T in K. a_R , b_R , and c_R are taken in Å at $T_R = 297$ K (see Tables A1–A3¹ for numerical values).

$$l(T) = x_1 U(T) + l_0 \quad (6)$$

and

$$l(T) = \frac{l_0 U(T)}{x_1 - x_2 U(T)} + l_0 \quad (7)$$

where l corresponds to either the a , b , or c lattice parameter, l_0 denotes the hypothetical lattice parameter at 0 K, and x_1 and x_2 are fitting parameters that are related to analogous axial terms given in Equations 3 and 4 (see Table 3).

Finally, using both first- and second-order Grüneisen approximations $V(T)$ dependencies were extrapolated to a temperature of ~2100 K, and, for the purposes of providing a simple description of the data and extrapolation, Equation 1 with $\alpha(T) = a_0 + a_1 T + a_2 T^{-1} + a_3 T^{-2}$ was fitted to these volumes for both phases (Table 4).

RESULTS AND DISCUSSION

Phase analyses and phase changes in wadsleyite and forsterite at high temperatures

Figure 1 shows schematic views of crystal structures of forsterite and wadsleyite. Typical diffraction patterns and Rietveld refinements for samples z626, z627, and forsterite are presented in Appendix Figures 1¹ and 2¹. A single-diffraction peak ($2\theta = \sim 18.8^\circ$) corresponding to a negligible amount of periclase was observed in sample z626 (PDF-2/card 37-415), whereas more pronounced amounts of periclase and forsterite were observed in diffraction patterns of z627. These impurity phases were included in the Rietveld fits yielding 1 and 5% of periclase (PDF-2/card 45-946) and forsterite, respectively, at room temperature (Appendix Fig. 1¹). We also checked for the existence of monoclinic distortions in wadsleyite samples (Smyth et al. 1997). The refined lattice parameters yield negligible monoclinic angles of 89.988(9) and 90.006(2)° for z626 and z627 samples and the volumes of monoclinic cells lie within 1σ of the orthorhombic cell volumes. We have, therefore, ignored the possibility of monoclinic distortion in our samples.

To obtain the absolute values for room-temperature volumes precisely, we have measured the diffraction pattern of z626 with an internal standard of powdered diamond mixed with the sample ($a = 3.5667$ Å, PDF-2/card 6-675). Sample z627 was not mixed with an internal standard but its measurement immediately after z626 ensured consistency in the experimental configuration. Note that the B2-beamline high-temperature setup provides for

extremely precise sample positioning (Knapp et al. 2004a), such that after initial calibration of the X-ray optical/detection systems with external LaB₆ standard, misalignment, and aberration are negligible between sample changes. Systematic errors in equipment displacement, which are not detectable by an application of external diffraction standard, results in the worse case in 4–5 estimated standard deviations (for instance, Allmann 2008).

The room-temperature volume of the wadsleyite sample z627 was found to be $\approx 0.25 \text{ \AA}^3$ larger than for z626 (Tables A1¹ and A2¹). This volume change is mainly caused by elongation of the *a*- and *b*- axes. The difference is approximately 10 times more than the estimated standard deviation obtained from Rietveld refinement, i.e., the difference is small but significant. Jacobsen et al. (2005) have demonstrated that the substitution of hydrogen (OH⁻) into the wadsleyite structure results in a sharp increase in the *b/a* lattice parameter ratio. This is not the case for these samples, and therefore, we can exclude the presence of hydrogen as a possible explanation. It cannot be excluded that some other contaminant was present in the sample to cause this volume dif-

TABLE 3. Axial thermal expansion parameters of wadsleyite and forsterite for the first- and second-order Grüneisen approximations

	l_0 (Å)	x_1	x_2	θ_0 (K)	R
Equation 6: Wadsleyite z626					
<i>a</i> (Å)	5.6961(9)	2.31(5)·10 ⁶		796(100)	0.9993705
<i>b</i> (Å)	11.4345(12)	4.46(9)·10 ⁶		939(82)	0.9994869
<i>c</i> (Å)	8.2416(9)	5.47(8)·10 ⁶		1067(59)	0.999697
Equation 6: Wadsleyite z627					
<i>a</i> (Å)	5.6976(8)	2.34(4)·10 ⁶		759(86)	0.9995405
<i>b</i> (Å)	11.4352(9)	4.42(5)·10 ⁶		788(57)	0.9994869
<i>c</i> (Å)	8.2412(6)	5.25(5)·10 ⁶		967(38)	0.999877
Equation 6: Forsterite					
<i>a</i> (Å)	4.7499(1)	4.258(6)·10 ⁶		853(10)	0.9999876
<i>b</i> (Å)	10.1788(4)	13.63(2)·10 ⁶		667(11)	0.9999854
<i>c</i> (Å)	5.9714(1)	7.183(8)·10 ⁶		662(10)	0.9999923
Equation 7: Wadsleyite z626					
<i>a</i> (Å)	5.699(1)	17.3(3)·10 ⁻¹⁷	-25(1)	1387(80)	0.999634
<i>b</i> (Å)	11.435(3)	25(2)·10 ⁻¹⁷	-3(2)	1004(101)	0.9994899
<i>c</i> (Å)	8.235(3)	20.0(4)·10 ⁻¹⁷	14(1)	538(78)	0.9998353
Equation 7: Wadsleyite z627					
<i>a</i> (Å)	5.698(1)	23.1(6)·10 ⁻¹⁷	-4(1)	858(99)	0.9995456
<i>b</i> (Å)	11.435(2)	26.6(4)·10 ⁻¹⁷	2(1)	736(67)	0.9997898
<i>c</i> (Å)	8.239(1)	17.6(1)·10 ⁻¹⁷	6.0(6)	761(49)	0.9999007
Equation 7: Forsterite					
<i>a</i> (Å)	4.7494(1)	11.59(8)·10 ⁻¹⁷	2.17(8)	765(10)	0.9999915
<i>b</i> (Å)	10.1785(6)	7.50(8)·10 ⁻¹⁷	0.14(6)	654(14)	0.9999854
<i>c</i> (Å)	5.9710(3)	8.42(7)·10 ⁻¹⁷	0.49(5)	630(11)	0.9999927

Note: To reproduce $l(T)$ dependencies according to Equations 6 and 7, use l_0 in m, and to get a final result in Å, multiply by a factor of 10¹⁰.

TABLE 4. Results of fits of Equation 1 with $\alpha(T) = a_0 + a_1T + a_2T^{-1} + a_3T^{-2}$ extrapolated to the ~ 2100 K volumes (extrapolations were performed on the basis of second-order Grüneisen approximation)

	a_0 (K ⁻¹)	a_1 (K ⁻²)	a_2	a_3 (K)
Extrapolation on the basis of second-order Grüneisen approximation				
Wadsleyite(z626)	3.02076·10 ⁻⁵	3.39486·10 ⁻⁹	-8.11328·10 ⁻⁴	-0.540578
Forsterite	3.45346·10 ⁻⁵	3.53839·10 ⁻⁹	1.11983·10 ⁻³	-0.66715

Notes: Measured V_R at $T_R = 298$ K was used (see Tables A1¹ and A3¹) at calculations. Note that such model is strictly overestimated, i.e., reveals large correlation between fitted parameters along with uncertainties comparable to their values and is given only for the purposes of providing a simple description of the data and extrapolation.

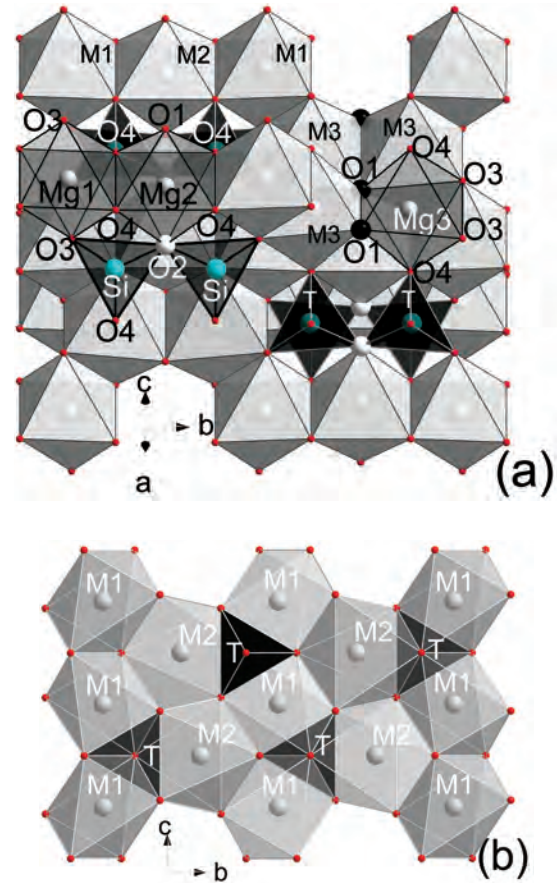


FIGURE 1. The view on the polyhedral representation of the wadsleyite crystal structure toward the (101) plane (a) and on the forsterite structure along the *a*-axis (b). Octahedral sites are denoted as M1, M2, and M3 and tetrahedral ones as T. The selected positions of non-silicate oxygen O1 and bridging O2 oxygen within Si₂O₇ dimers of wadsleyite are depicted by larger spheres.

ference. However, if so, it was unclear as to what the contaminant would be because only high-purity oxides were employed and the samples were encapsulate during the synthesis. A further possibility is that a difference in silica activity in the samples caused a variation in possible Mg-Si disorder. Sample z627, with a slightly larger volume coexisted with periclase and therefore, plausibly experienced a lower silica activity compared to sample z626. Although Stebbins et al. (2009) found no evidence for octahedral Si in wadsleyite from nuclear magnetic resonance measurements, the sample studied also contained an excess of MgO and therefore silica activity was buffered at low levels. The lower volume of sample z626 might potentially arise from higher silica activity stabilizing small amounts of octahedrally coordinated Si. The proportions of wadsleyite, forsterite, and periclase in sample z627 were temperature independent up to 1058 K. At 1110 K, wadsleyite began to transform back to forsterite and the proportion decreased to 91%. At 1163 K, the highest temperature achieved, the wadsleyite proportion dropped to 44%. After cooling the furnace to room temperature for approximately 26 min, only 11% wadsleyite was detected in the recovered sample (Appendix Fig. 2¹). Changes of the microstructure were

also observed throughout the phase transition, which caused diffraction lines to broaden significantly. This broadening was also present in the pattern measured after temperature treatment. As a result, analyses above 1084 K were excluded from fitting.

To avoid decomposition of wadsleyite to forsterite, the upper temperature was limited to 1084 K for the second experiment on sample z626. No sign of wadsleyite transformation to forsterite was observed for the sample z626 high-temperature cycle and the volume of the recovered wadsleyite sample, $538.213(13) \text{ \AA}^3$, was within the estimated standard deviation of the starting powder. Suzuki et al. (1980) reported wadsleyite back transformation to commence promptly at 1173 K, a similar temperature to that found in our study. Inoue et al. (2004) reported wadsleyite back transformation at the somewhat lower temperature of 1073 K. Ye et al. (2009) reported that single crystals of anhydrous wadsleyite became polycrystalline at 859 K, whereas Tsukimura et al. (1988), in their experiments on single crystals, observed the onset of transformation at approximately 850 K. These differences in temperature are consistent with the kinetics of the back reaction determined by Reynard et al. (1996), because single-crystal studies require samples to be held for many hours at a single temperature, whereas powder measurements, especially those performed using synchrotron sources, can be completed in a matter of minutes.

Thermal expansion of wadsleyite and forsterite

Lattice parameters of wadsleyite (samples z626 and z627) and forsterite at elevated temperatures are summarized in Appendix Tables 1¹, 2¹, and 3¹. Temperature dependency of unit-cell parameters and relative expansion $\{\delta x(T) = 100\% \times [x(T) - x(298 \text{ K})]/x(298 \text{ K})\}$, where x 's are unit-cell parameters a , b , and c , respectively are presented in Figures 2 and 3, and thermal expansion parameters are summarized in Tables 1–3.

The relative expansions for the a , b , and c axes of forsterite

are 0.97, 1.48, and 1.34% at 1313 K, respectively, yielding a volumetric relative expansion of 3.84% at this temperature (Fig. 3). Such pronounced anisotropy in thermal expansion with a stiffer a -axis agrees well with several references summarized in Smyth et al. (2000). There is no significant difference between the relative expansions determined for the two wadsleyite samples (Fig. 2). The relative expansions of the a and b axes at 1084 K are very similar 0.67 and 0.63%, respectively, whereas the c axis expansion is 1.06%, indicating pronounced anisotropy in the expansion with $\delta c/\delta a = 1.58$ and $\delta c/\delta b = 1.68$. These results are consistent with those of Suzuki et al. (1980). The thermal expansion is largest along the c direction, which has also been shown to display the highest linear compressibility (e.g., Holl et al. 2008; Downs et al. 1996). Correlations between directions displaying the highest linear expansion and compressibility are common; however, there are exceptions, such as in the mineral diomignite, $\text{Li}_2\text{B}_2\text{O}_7$, which contains B_2O_7 dimers similar to silicate dimers in wadsleyite (see Trots et al. 2011 and references therein).

As shown in Figure 4a, over the range of temperatures investigated, the $V(T)$ data for forsterite are in good agreement with the works of Ye et al. (2009) and Hazen (1976) [(based on the work of Smyth and Hazen (1973))]. The measurements of Suzuki et al. (1983) show a slightly greater curvature compared with our data whereas data from Bouhifd et al. (1996) plot consistently below our measurements, although in agreement within error up to approximately 1000 K. First- and second-order fits employing the Grüneisen approximation are shown in Figure 4b. Values for K_0 and K' of forsterite were constrained in the fitting procedure using the measurements of Downs et al. (1996). The resulting parameters are reported in Table 1. Values for θ_D and γ from the first-order fit are in good agreement with values from the literature determined independently from elasticity measurements, which are in the range $\theta_D = 732\text{--}760 \text{ K}$ (Suzuki et al. 1983; Isaak et al. 1989) and $\gamma = 1.1\text{--}1.29$ (Anderson et al. 1995; Suzuki et

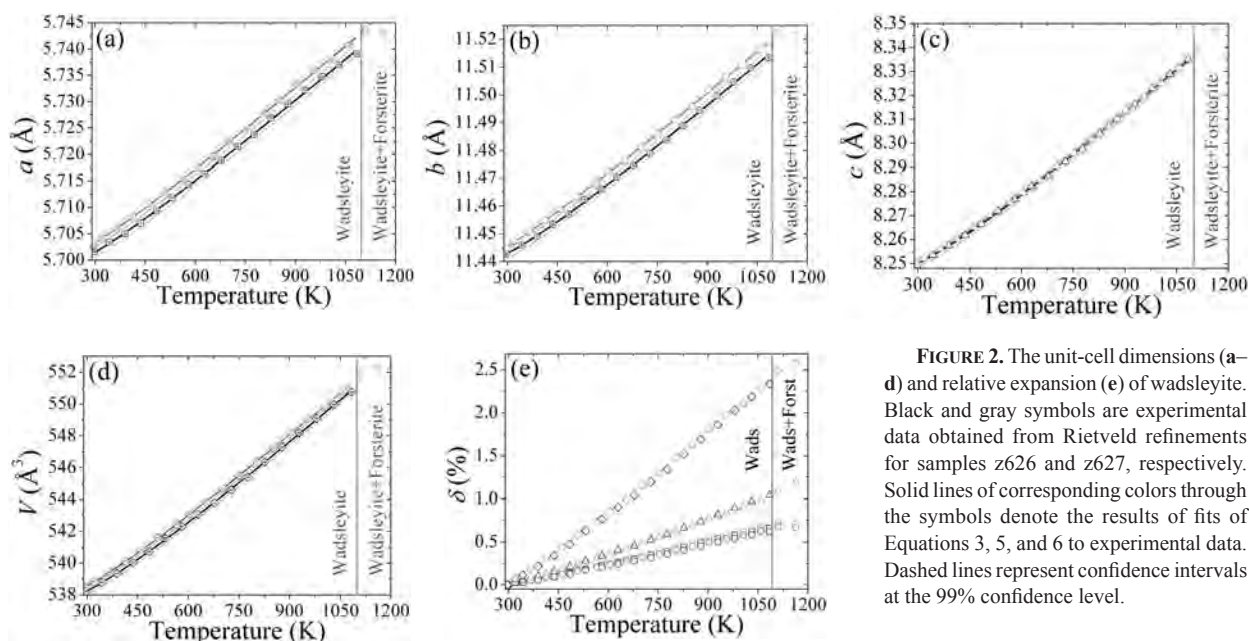


FIGURE 2. The unit-cell dimensions (a–d) and relative expansion (e) of wadsleyite. Black and gray symbols are experimental data obtained from Rietveld refinements for samples z626 and z627, respectively. Solid lines of corresponding colors through the symbols denote the results of fits of Equations 3, 5, and 6 to experimental data. Dashed lines represent confidence intervals at the 99% confidence level.

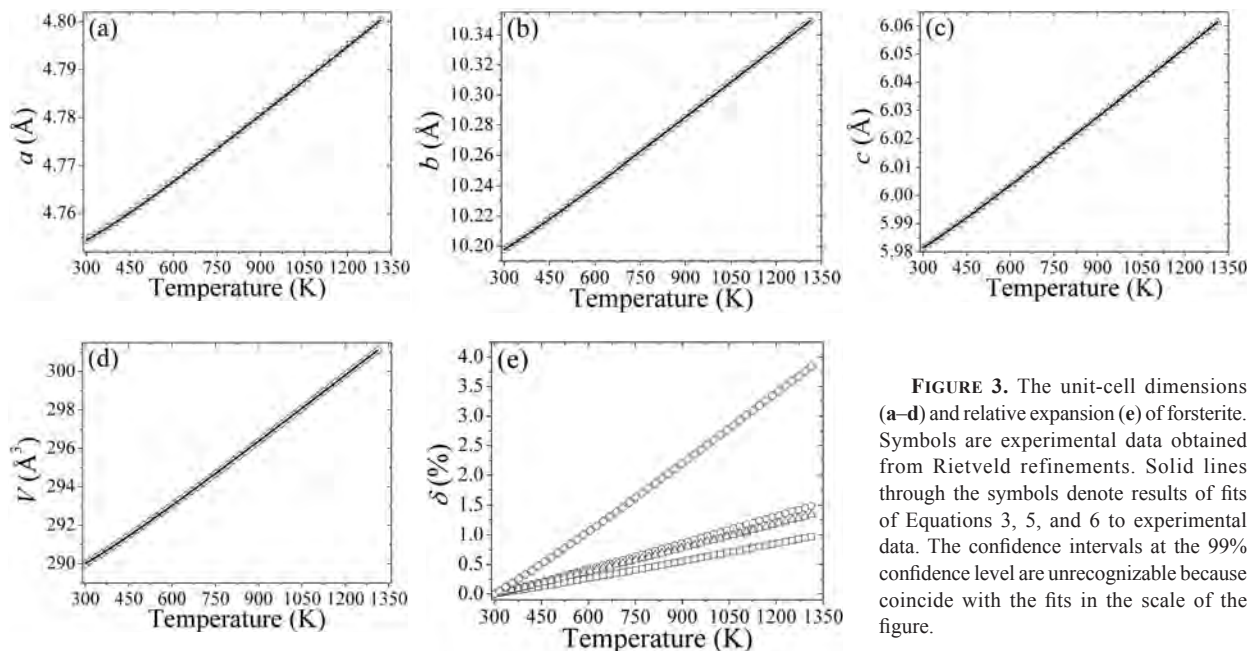


FIGURE 3. The unit-cell dimensions (a–d) and relative expansion (e) of forsterite. Symbols are experimental data obtained from Rietveld refinements. Solid lines through the symbols denote results of fits of Equations 3, 5, and 6 to experimental data. The confidence intervals at the 99% confidence level are unrecognizable because coincide with the fits in the scale of the figure.

al. 1983). On the other hand, fitting using the second-order approximation results in an anomalously low value for θ_D of 483 K compared to independent estimates. Residuals indicate that both approximations fit the data to a very similar level.

In Figure 4b, extrapolations of both first- and second-order fits are compared with literature equations of state up to the melting temperature of ~ 2150 K. The two fitting curves diverge above 1600 K and predict volumes that differ by 0.4% at the melting temperature. Interestingly, the first-order approximation returns to perfect agreement with the measurements of Bouhifd et al. (1996) at the melting point, although, given the larger deviations at lower temperature, this likely has no significance. In general, the best agreement is found with the equation of state of Holland and Powell (2011) who employed data of Hazen (1976) and Kajiyoshi (1986). The equations of Stixrude and Lithgow-Bertelloni (2005) and Fabrichnaya et al. (2004) are in better agreement with the data of Bouhifd et al. (1996) on which they are based. The simple linear equation of Ye et al. (2009) is unsuitable for extrapolation.

The current data on wadsleyite are compared in Figure 5a with previous studies. The measurements of Ye et al. (2009) are in excellent agreement with this study and the results of Suzuki et al. (1980) are in good agreement. Data reported by Inoue et al. (2004) on anhydrous wadsleyite are consistently higher than those measured in this study and show more scatter. Fits employing first- and second-order Grüneisen approximations are shown in Figure 5b. Literature values for K_0 and K' of wadsleyite were taken from Angel et al. (2001) and the fitting parameters are given in Table 1. Refined θ_D values of 980(55) and 816(50) K for first- and second-order fits for sample z626 are in good agreement with an independent literature value of 993 K (Watanabe 1982), which is mean thermal Debye temperature between 350 and 700 K obtained by calorimetric measurements. Furthermore,

according to Suzuki et al. (1980), the value of 830 K for acoustic Debye temperature was estimated based on the bulk modulus of wadsleyite reported by Mizukami et al. (1975) [see also Suzuki et al. (1980) and references therein]. The refined values of γ for both fits are also in good agreement with other estimates, i.e., 1.29 (Watanabe 1982). Although refined θ_D values for sample z627 are lower than those of z626, they are still in agreement within the uncertainties. Data for sample z627 also lie within the confidence intervals of sample z626 and vice versa. Thus, the $V(T)/V_R$ data are displayed by the lower and upper confidence boundaries for samples z626 and z627 in Figure 5.

Figure 5b shows extrapolations of the two wadsleyite fitting curves to 2000 K and a comparison with other equations. The first- and second-order equations diverge above 1600 K and are different by approximately 0.4% at the highest temperature. Over the range of measurements there is excellent agreement with the equations of state of Holland and Powell (2011) and Stixrude and Lithgow-Bertelloni (2005), with the former equation in better agreement with the extrapolations made using Grüneisen theory. The agreement with the proposed equation of state of Katsura et al. (2009) is also very good, whereas the constant thermal expansion term proposed by Inoue et al. (2004) results in volumes up to 0.5% higher over most of the temperature range examined. The equation of Li et al. (2001) determined using high-pressure data reproduces room-pressure volumes poorly and the equation of Ye et al. (2009) is likely unsuitable for extrapolation.

As hydrous Mg_2SiO_4 polymorphs are more compressible and expandable at ambient pressure than their anhydrous counterparts, one would expect a decrease in the Debye temperature of hydrous samples (Debye temperature can be defined as an estimate of magnitude of phonon frequencies in crystal). To test this, the first- and second-order Grüneisen approximations were employed to model $V(T)$ dependencies of hydrous forster-

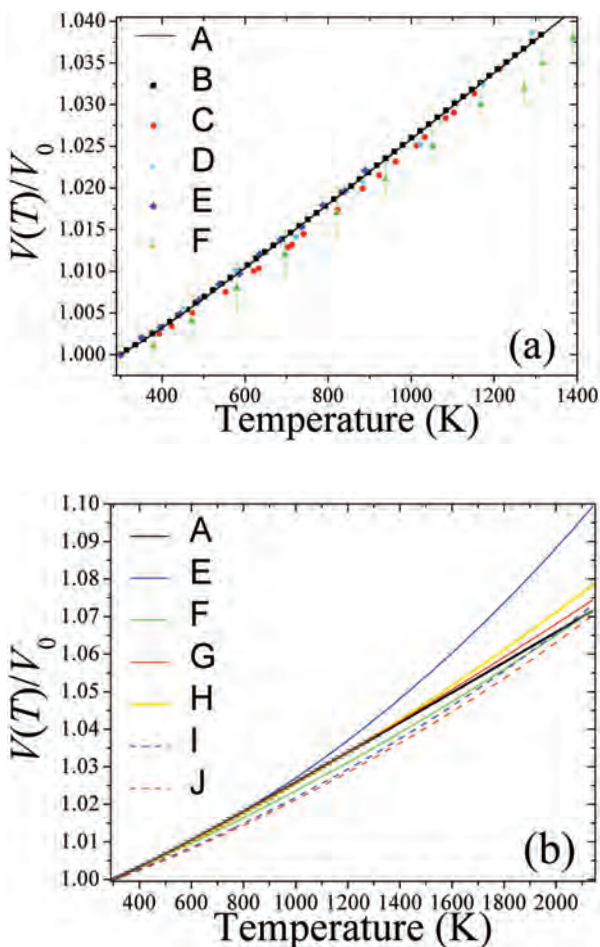


FIGURE 4. The $V(T)/V_R$ dependency of forsterite compared with the experimental results (a) and results of extrapolation (b) up to 2150 K (see text for details). A = first-order Grüneisen approximation, B = experimental data of this work, C = Suzuki et al. (1983), D = Hazen (1976), E = Ye et al. (2009), F = Bouhifd et al. (1996), G = second-order Grüneisen approximation, H = Holland and Powell (2011), I = Fabrichnaya et al. (2004), J = Stixrude and Lithgow-Bertelloni (2005).

ite, wadsleyite, and ringwoodite (Ye et al. 2009). A systematic increase of around 100–150 K in the Debye temperature of hydrous minerals was observed, however. On the other hand, the analysis of acoustic Debye temperatures, which were derived for hydrous and anhydrous samples from references Mao et al. (2008, 2010), reveals decrease in acoustic Debye temperature with increase of hydration degree.

High-temperature structural variations in wadsleyite

High-temperature structural variations of forsterite were comprehensively investigated by Hazen (1976) and are not examined here. Structural parameters of wadsleyite determined by Rietveld refinements at selected temperatures are documented in Table A4¹ and selected distances and angles for both samples z626 and z627 are illustrated in Appendix Figures 3¹ and 4¹. There is a small difference between interatomic distances/angles of the two samples but their trends with temperature are identical.

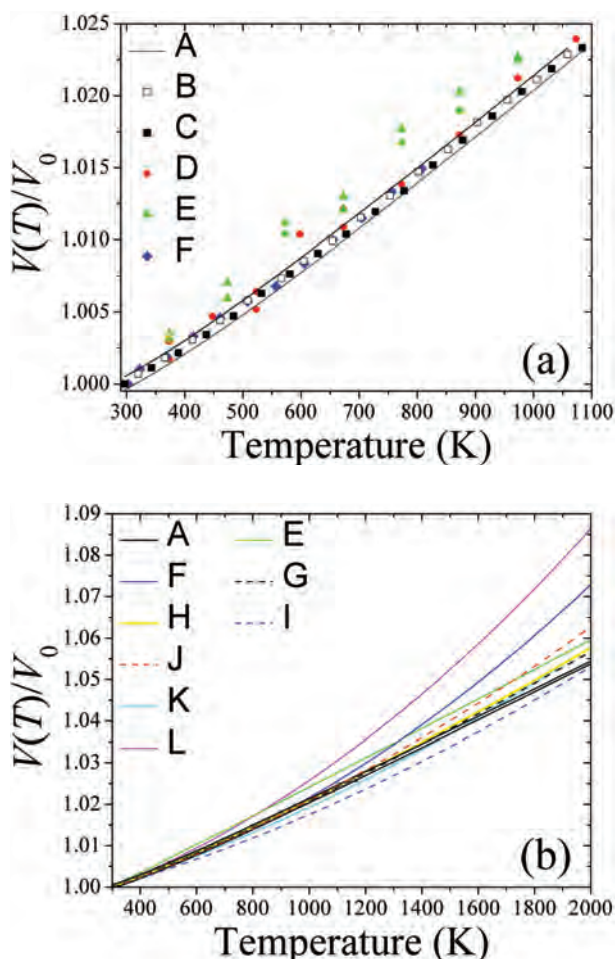


FIGURE 5. The $V(T)/V_R$ dependency of wadsleyite compared with the experimental results (a) and results of extrapolation (b) up to 2000 K (see text for details). A = confidence interval for first-order Grüneisen approximation (see text for details), B = experimental data for z627, C = experimental data for z626, D = Suzuki et al. (1980), E = Inoue et al. (2004), F = Ye et al. (2009), G = second-order Grüneisen approximation, H = Holland and Powell (2011), I = Fabrichnaya et al. (2004), J = Stixrude and Lithgow-Bertelloni (2005), K = Katsura et al. (2009), L = Li et al. (2001).

Extensive edge-sharing of octahedra in the wadsleyite structure (Fig. 1) limits the accommodation of expansion or compression by means of cation-oxygen-cation angle bending. The only relatively flexible angle in the structure is the angle between the Si and the bridging oxygen of the Si_2O_7 dimers. This angle is observed to increase with temperature (Appendix¹ Fig. 4) and decrease with pressure (Hazen et al. 2000).

Changes in tetrahedral bond distances and tetrahedral volume from room temperature up to 1083 K are practically negligible. Therefore, the SiO_4 tetrahedra behave as rigid structural units both during expansion, at least up to the temperatures investigated here, and during compression up to 10 GPa (Hazen et al. 2000). The temperature independency of tetrahedral volumes was also observed for both hydrous and anhydrous wadsleyite by Ye et al. (2011), up to ~725 K. The expansion of the wadsleyite

structure is, therefore, mainly accommodated by expansion of the octahedral sites. The individual Mg-O bonds expand differently, with the shorter bonds expanding more than the longest. The only exception is the Mg3-O1 distances, which, in spite of being the shortest at room temperature (2.008 Å), increase only 0.8% up to 1083 K. This is likely due to the extensive edge sharing of the M3 octahedra along the O1-O1 edges. There is a major difference between the expansion and the compression behavior of wadsleyite: the axial anisotropy with the *c*-axis is both more expandable and more compressible than the other two axes and cannot be related to the behavior of the same bond lengths. In fact, while Mg1-O3, Mg2-O2, and Mg3-O3, which are roughly parallel to the *c* axis, are the most compressible bonds (Hazen et al. 2000), they experience limited or practically negligible expansion (Appendix Fig. 3). With temperature increase, the Mg2-O1 bond appears to be mainly responsible for the axial anisotropy, which is roughly parallel to the *c* axis, the most expandable direction (2.4% up to 1083 K).

Plots of octahedral volumes vs. temperature imply a slightly greater expansion for V_{M1} , however, this may not be justified given the scatter of the data (Appendix Fig. 3f). The results of Ye et al. (2011), which are less scattered due to the use of single-crystal diffraction, reveal almost the same expansion among V_{M1} , V_{M2} , and V_{M3} for both hydrous and anhydrous wadsleyite. This is consistent with the same compression of the three octahedral sites reported in Hazen et al. (2000).

ACKNOWLEDGMENTS

We acknowledge the support of the ERC advanced grant no. 227893 “DEEP” funded through the EC 7th Framework Programme. X-ray diffraction measurements with synchrotron radiation were carried out during beamtime allocated to Project I-20090287 at HASYLAB/DESY.

REFERENCES CITED

- Allmann, R. (2008) General data reduction. In R.E. Dinnebier, S.J.L. Billinge, Eds., *Powder Diffraction: Theory and Practice*, 605 p. The Royal Society of Chemistry, Cambridge CB4 0WF, U.K.
- Anderson, O.L., Masuda, K., and Isaak, D.G. (1995) A new thermodynamic approach for high-pressure physics. *Physics of the Earth and Planetary Interiors*, 91, 3–16.
- Angel, R.J., Frost, D.J., Ross, N.L., and Hemley, R. (2001) Stabilities and equations of state of dense hydrous magnesium silicates. *Physics of the Earth and Planetary Interiors*, 127, 181–196.
- Bouhifd, M.A., Andrau It, D., Fiquet, G., and Richet, P. (1996) Thermal expansion of forsterite up to the melting point. *Geophysical Research Letters*, 23, 1143–1146.
- Downs, R.T., Zha, C.-S., Duffy, T.S., and Finger, L.W. (1996) The equation of state of forsterite to 17.2 GPa and effects of pressure media. *American Mineralogist*, 81, 51–55.
- Fabrichnaya, O., Saxena, S.K., Richet, P., Westrum, E.F. (2004) Thermodynamic data on solid phases in the system: MgO–FeO–Fe₂O₃–Al₂O₃–SiO₂, 198 p. Springer, Berlin.
- Fei, Y. and Saxena, S.K. (1986) A thermochemical data base for phase equilibria in the system Fe–Mg–Si–O at high pressure and temperature. *Physics and Chemistry of Minerals*, 13, 311–324.
- Fei, Y. (1995) Thermal expansion. In T.J. Ahrens, Ed., *Mineral physics and crystallography—A handbook of physical constants*, 354 p. AGU reference shelf 2, AGU, Washington, D.C.
- Fortes, A.D., Wood, I.G., Vocadlo, L., Brand, H.E.A., and Knight, K.S. (2007) Crystal structures and thermal expansion of α -MgSO₄ and β -MgSO₄ from 4.2 to 300 K by powder neutron diffraction. *Journal of Applied Crystallography*, 40, 761–770.
- Frost, D.J., Poe, B.T., Tronnes, R.G., Liebske, C., Duba, A., and Rubie, D.C. (2004) A new large-volume multianvil system. *Physics of the Earth and Planetary Interiors*, 143–144, 507–514.
- Gillet, P., Richet, P., Guyot, F., and Fiquet, G. (1991) High-temperature thermodynamic properties of forsterite. *Journal of Geophysical Research, Solid Earth*, 96, 11805–11816.
- Hazen, R.M. (1976) Effects of temperature and pressure on the crystal structure of forsterite. *American Mineralogist*, 61, 1280–1293.
- Hazen, R.M., Weinberger, M.B., Yang, H., and Prewitt, C.T. (2000) Comparative high-pressure crystal chemistry of wadsleyite, β -(Mg_{1-x}Fe_x)₂SiO₄, with x = 0 and 0.25. *American Mineralogist*, 85, 770–777.
- Holl, C.M., Smyth, J.R., Jacobsen, S.D., and Frost, D.J. (2008) Effects of hydration on the structure and compressibility of wadsleyite, β -(Mg₂SiO₄). *American Mineralogist*, 93, 598–607.
- Holland, T.J.B. and Powell, R. (2011) An improved and extended internally consistent thermodynamic dataset for phases of petrological interest, involving a new equation of state for solids. *Journal of Metamorphic Geology*, 29, 333–383.
- Inoue, T., Tanimoto, Y., Irifune, T., Suzuki, T., Fukui, H., and Ohtaka, O. (2004) Thermal expansion of wadsleyite, ringwoodite, hydrous wadsleyite and hydrous ringwoodite. *Physics of the Earth and Planetary Interiors*, 143–144, 279–290.
- Isaak, D.G., Anderson, O.L., Goto, T., and Suzuki, I. (1989) Elasticity of single-crystal forsterite measured to 1700K. *Journal of Geophysical Research-Solid Earth*, 94, 5895–5906.
- Jacobsen, S.D., Demouchy, S., Frost, D.J., Boffa Ballaran, T., and Kung, J. (2005) A systematic study of OH in hydrous wadsleyite from polarized FTIR spectroscopy and single-crystal X-ray diffraction: Oxygen sites for hydrogen storage in Earth's interior. *American Mineralogist*, 90, 61–70.
- Kajiyoshi, K. (1986) High-temperature equation of state for mantle minerals and their anharmonic properties. M.S. thesis, Okayama University, Japan (as quoted by Isaak et al. 1989).
- Katsura, T., Shatskiy, A., Manthilake, M.A.G.M., Zhai, S., Yamazaki, D., Matsuzaki, T., Yoshino, T., Yoneda, A., Ito, E., Sugita, M., Tomioka, N., Nozawa, A., and Funakoshi, K.-I. (2009) *P–V–T* relations of wadsleyite determined by in situ X-ray diffraction in a large-volume high-pressure apparatus. *Geophysical Research Letters*, 36, L11307.
- Knapp, M., Baecht, C., Ehrenberg, H., and Fuess, H. (2004a) The synchrotron powder diffractometer at beamline B2 at HASYLAB/DESY: status and capabilities. *Journal of Synchrotron Radiation*, 11, 328–334.
- Knapp, M., Joco, V., Baecht, C., Brecht, H.H., Berghäuser, A., Ehrenberg, H., von Seggern, H., and Fuess, H. (2004b) Position-sensitive detector system OBI for high resolution X-ray powder diffraction using on-site readable image plates. *Nuclear Instruments and Methods in Physics Research Section A: Accelerators, Spectrometers, Detectors and Associated*, 521, 565–570.
- Larson, A.C. and von Dreele, R.B. (2004) General structure analysis system (GSAS). Los Alamos National Laboratory Report, LAUR 86-748.
- Li, B., Liebermann, R.C., and Weidner, D.J. (2001) *P–V–V_T–V_S–T* measurements on wadsleyite to 7 GPa and 873 K: implications for the 410–km seismic discontinuity. *Journal of Geophysical Research—Solid Earth*, 106, 30579–30591.
- Lindsay-Scott, A., Wood, I.G., and Dobson, D.P. (2007) Thermal expansion of CaIrO₃ determined by X-ray powder diffraction. *Physics of the Earth and Planetary Interiors*, 162, 140–148.
- Mao, Z., Jacobsen, S.D., Jiang, F.M., Smyth, J.R., Holl, C.M., Frost, D.J., and Duffy T.S. (2008) Single crystal elasticity of wadsleyites, β -Mg₂SiO₄, containing 0.37–1.66 wt.% H₂O. *Earth and Planetary Science Letters*, 268, 540–549.
- Mao, Z., Jacobsen, S.D., Jiang, F., Smyth, J.R., Holl, C.M., Frost, D.J., and Duffy T.S. (2010) Velocity crossover between hydrous and anhydrous forsterite at high pressures. *Earth and Planetary Science Letters*, 293, 250–258.
- Matsui, T. and Manghnani, M.H. (1985) Thermal expansion of single-crystal forsterite to 1023 K by Fizeau interferometry. *Physics and Chemistry of Minerals*, 12, 201–210.
- Mizukami, S., Ohtani, A., Kawai, N., and Ito, E. (1975) High-pressure X-ray diffraction studies of β - and γ -Mg₂SiO₄. *Physics of the Earth and Planetary Interiors*, 10, 177–182.
- Pathak, P.D. and Vasavada, N.G. (1970) Thermal expansion of NaCl, KCl and CsBr by X-ray diffraction and the law of corresponding states. *Acta Crystallographica*, A26, 655–658.
- Reynard, B., Takir, F., Guyot, F., Gwanmesia, G.D., Liebermann, R.C., and Gillet, P. (1996) High-temperature Raman spectroscopic and X-ray diffraction study of β -Mg₂SiO₄: insights into its high-temperature thermodynamic properties and the β - to α -phase-transformation mechanism and kinetics. *American Mineralogist*, 81, 585–594.
- Ringwood, A.E. (1975) *Composition and Petrology of the Earth's Mantle*, 672 p. McGraw-Hill, New York.
- Rodriguez-Carvajal, J. (1993) Recent advances in magnetic structure determination by neutron powder diffraction. *Physica B*, 192, 55–69.
- Senyshyn, A., Trots, D.M., Engel, J.M., Vasylechko, L., Ehrenberg, H., Hansen, T., Berkowski, M., and Fuess, H. (2009) Anomalous thermal expansion in rare-earth gallium perovskites: a comprehensive powder diffraction study. *Journal of Physics: Condensed Matter*, 21, 145405.
- Skinner, B.J. (1962) Thermal expansion of ten minerals. U.S. Geological Survey Professional Paper, 450D, p. 109–112 (as quoted by Bouhifd et al. 1996).
- Smyth, J.R. and Hazen, R.M. (1973) Crystal structures of forsterite and hortonolite at several temperatures up to 900°C. *American Mineralogist*, 58, 588–593.
- Smyth, J.R., Kawamoto, T., Jacobsen, S.D., Swope, R. J., Hervig, R.L. Hol-

- loway, J.R. (1997) Crystal structure of monoclinic hydrous wadsleyite [β -(Mg,Fe) $_2$ SiO $_4$]. *American Mineralogist*, 82, 270–275.
- Smyth, J.R., Jacobsen, S.D., and Hazen R.M. (2000) Comparative crystal chemistry of orthosilicate minerals. In R.M. Hazen and R.T. Downs, Eds., *High-temperature and High-pressure Crystal Chemistry*, vol. 41, p. 187–209. *Reviews in Mineralogy and Geochemistry*, Mineralogical Society of America, Chantilly, Virginia.
- Stebbins, J.F., Panero, W.R., Smyth, J.R., and Frost, D.J. (2009) Forsterite, wadsleyite, and ringwoodite (Mg $_2$ SiO $_4$) 29 Si NMR constraints on structural disorder and effects of paramagnetic impurity ions. *American Mineralogist*, 94, 626–629.
- Stixrude, L. and Lithgow-Bertelloni, C. (2005) Thermodynamics of mantle minerals – I. Physical properties. *Geophysical Journal International*, 162, 610–632.
- Suzuki, I., Ohtani, E., and Kumazawa, M. (1980) Thermal expansion of modified spinel, β -Mg $_2$ SiO $_4$. *Journal of Physics of the Earth*, 28, 273–280.
- Suzuki, I., Anderson, O.L., and Sumino, Y. (1983) Elastic properties of a single-crystal forsterite Mg $_2$ SiO $_4$ up to 1200 K. *Physics and Chemistry of Minerals*, 10, 38–46.
- Suzuki, I., Takei, H., and Anderson, O.L. (1984) Thermal expansion of forsterite, Mg $_2$ SiO $_4$. In T.A. Hahn, Ed., *Thermal Expansion* 8, p. 79–88. Plenum Press, New York.
- Takeuchi, Y., Yamanaka T., Haga, N., and Hirano, M. (1984) High-temperature crystallography of olivines and spinels. In I. Sunagawa, Ed., *Materials Science for the Earth's Interior*, p. 191–231 (as quoted by Bouhifd et al. 1996). Terra, Tokyo.
- Tsukimura, K., Sato-Sorensen, Y., Ghose, S., and Sawamoto, H. (1988) High-temperature single crystal study of β -Mg $_2$ SiO $_4$. *EOS Transactions*, 69, 498.
- Trots, D.M., Senyshyn, A., Vasylechko, L., Niewa, R., Vad, T., Mikhailik, V.B., and Kraus, H. (2009) Crystal structure of ZnWO $_4$ scintillator material in the range of 3–1423 K. *Journal of Physics: Condensed Matter*, 21, 325402.
- Trots, D.M., Kurnosov, A., Vasylechko, L., Berkowski, M., Boffa Ballaran, T., and Frost, D.J. (2011) Elasticity and equation of state of Li $_2$ B $_4$ O $_7$. *Physics and Chemistry of Minerals*, 38, 561–567.
- Vočadlo, L., Knight, K.S., Price, G.D., and Wood, I.G. (2002) Thermal expansion and crystal structure of FeSi between 4 and 1173 K determined by time-of-flight neutron powder diffraction. *Physics and Chemistry of Minerals*, 29, 132–139.
- Vokurka, K. and Rieder, M. (1987) Thermal expansion and excess volumes of synthetic olivines on the Mg $_2$ SiO $_4$ -Ni $_2$ SiO $_4$ join. *Neues Jahrbuch für Mineralogie-Monatshefte*, 3, 97–106.
- Wallace, D.C. (1998) *Thermodynamics of Crystals*, 512 p. Dover, New York.
- Watanabe, H. (1982) Thermochemical properties of synthetic high-pressure compounds relevant to the Earth's mantle. In S. Akimoto and M.H. Manghnani, Eds., *High-Pressure Research in Geophysics*, p. 441–464. Center for Academic Publications Japan, Tokyo.
- White, G.K., Roberts, R.B., and Collins, J.G. (1985) Thermal properties and Grüneisen functions of forsterite, Mg $_2$ SiO $_4$. *High Temperatures-High Pressures*, 17, 61–66.
- Ye, Y., Schwering, R.A., and Smyth, J.R. (2009) Effects of hydration on thermal expansion of forsterite, wadsleyite, and ringwoodite at ambient pressure. *American Mineralogist*, 94, 899–904.
- Ye, Y., Smyth, J.R., and Frost, D.J. (2011) Structural study of the coherent dehydration of wadsleyite. *American Mineralogist*, 96, 1760–1767.

MANUSCRIPT RECEIVED SEPTEMBER 4, 2011

MANUSCRIPT ACCEPTED JUNE 29, 2012

MANUSCRIPT HANDLED BY BORIANA MIHAILOVA

```

data_wadsleyite
_audit_creation_method 'Created with CONVERT.DLL (www.crystalimpact.com)'
_audit_creation_date 2011-09-04
_audit_update_record 2011-09-04
_journal_codem_ASTM ?
_journal_year ?
_journal_volume ?
_journal_page_first ?
_journal_page_last ?
_publ_author_name '?,'
_publ_section_title
;
' 297'
;
_chemical_formula_sum 'Mg2 Si O4'
_chemical_formula_structural 'Mg16Si8O32'
_chemical_formula_analytical 'Mg2SiO4'
_chemical_name_common
;
wadsleyite
;
_chemical_compound_source
;
Multianvil facility at BGI
;
_chemical_formula_weight 140.693
_cell_length_a 5.7016(1)
_cell_length_b 11.4427(2)
_cell_length_c 8.2491(1)
_cell_angle_alpha 90.000
_cell_angle_beta 90.000
_cell_angle_gamma 90.000
_cell_volume 538.2(0)
_cell_formula_units_Z 8
_symmetry_int_tables_number 74
_symmetry_space_group_name_H-M 'I m m a'
_symmetry_space_group_name_Hall '-I_2b_2'

loop_
_symmetry_equiv_pos_site_id
_symmetry_equiv_pos_as_xyz
1 x,y,z
2 -x,0.500-y,z
3 x,-y,-z
4 -x,0.500+y,-z
5 -x,-y,-z
6 x,0.500+y,-z
7 -x,y,z
8 x,0.500-y,z
9 0.500+x,0.500+y,0.500+z
10 0.500-x,1.000-y,0.500+z
11 0.500+x,0.500-y,0.500-z
12 0.500-x,1.000+y,0.500-z
13 0.500-x,0.500-y,0.500-z
14 0.500+x,1.000+y,0.500-z
15 0.500-x,0.500+y,0.500+z

```

16 0.500+x,1.000-y,0.500+z

```

loop_
_atom_type_symbol
_atom_type_oxidation_number
_atom_type_radius_bond
Mg      ?      1.200
Si      ?      1.200
O       ?      1.200

```

```

loop_
_atom_site_label
_atom_site_type_symbol
_atom_site_fract_x
_atom_site_fract_y
_atom_site_fract_z
_atom_site_occupancy
_atom_site_symmetry_multiplicity
_atom_site_Wyckoff_symbol
_atom_site_attached_hydrogens
_atom_site_calc_flag
_atom_site_thermal_displace_type
_atom_site_u_iso_or_equiv
Mg1 Mg  0.0000  0.0000  0.0000  1.000 4 a ? d Biso  0.12(4)
Mg2 Mg  0.0000  0.2500  0.9726(4)  1.000 4 e ? d Biso  0.12(4)
Mg3 Mg  0.2500  0.1286(4)  0.2500  1.000 8 g ? d Biso  0.12(4)
Si1 Si  0.0000  0.1187(3)  0.6175(4)  1.000 8 h ? d Biso  0.12(4)
O1  O   0.0000  0.2500  0.2177(9)  1.000 4 e ? d Uiso  0.12(4)
O2  O   0.0000  0.2500  0.7179(9)  1.000 4 e ? d Uiso  0.12(4)
O3  O   0.0000  0.9929(4)  0.2548(9)  1.000 8 h ? d Uiso  0.12(4)
O4  O   0.2624(5)  0.1227(12)  0.9945(4)  1.000 16 j ? d Uiso  0.12(4)

```

```

data_Wadsleyite
_audit_creation_method 'Created with CONVERT.DLL (www.crystalimpact.com)'
_audit_creation_date 2011-09-04
_audit_update_record 2011-09-04
_journal_codenn_ASTM ?
_journal_year ?
_journal_volume ?
_journal_page_first ?
_journal_page_last ?
_publ_author_name '?,'
_publ_section_title
;
' 728'
;
_chemical_formula_sum 'Mg2 Si O4'
_chemical_formula_structural 'Mg16Si8O32'
_chemical_formula_analytical 'Mg2SiO4'
_chemical_name_common
;
wadsleyite
;
_chemical_compound_source
;
Multianvil facility at BGI
;
_chemical_formula_weight 140.693
_cell_length_a 5.7214(1)
_cell_length_b 11.4789(2)
_cell_length_c 8.2924(2)
_cell_angle_alpha 90.000
_cell_angle_beta 90.000
_cell_angle_gamma 90.000
_cell_volume 544.6(0)
_cell_formula_units_Z 8
_symmetry_int_tables_number 74
_symmetry_space_group_name_H-M 'I m m a'
_symmetry_space_group_name_Hall '-I_2b_2'

loop_
_symmetry_equiv_pos_site_id
_symmetry_equiv_pos_as_xyz
1 x,y,z
2 -x,0.500-y,z
3 x,-y,-z
4 -x,0.500+y,-z
5 -x,-y,-z
6 x,0.500+y,-z
7 -x,y,z
8 x,0.500-y,z
9 0.500+x,0.500+y,0.500+z
10 0.500-x,1.000-y,0.500+z
11 0.500+x,0.500-y,0.500-z
12 0.500-x,1.000+y,0.500-z
13 0.500-x,0.500-y,0.500-z
14 0.500+x,1.000+y,0.500-z
15 0.500-x,0.500+y,0.500+z

```

16 0.500+x,1.000-y,0.500+z

```

loop_
_atom_type_symbol
_atom_type_oxidation_number
_atom_type_radius_bond
Mg      ?      1.200
Si      ?      1.200
O       ?      1.200

```

```

loop_
_atom_site_label
_atom_site_type_symbol
_atom_site_fract_x
_atom_site_fract_y
_atom_site_fract_z
_atom_site_occupancy
_atom_site_symmetry_multiplicity
_atom_site_Wyckoff_symbol
_atom_site_attached_hydrogens
_atom_site_calc_flag
_atom_site_thermal_displace_type
_atom_site_u_iso_or_equiv
Mg1 Mg  0.0000  0.0000  0.0000  1.000  4  a  ?  d  Biso  0.23(3)
Mg2 Mg  0.0000  0.2500  0.9711(5)  1.000  4  e  ?  d  Biso  0.23(3)
Mg3 Mg  0.2500  0.1280(5)  0.2500  1.000  8  g  ?  d  Biso  0.23(3)
Si1 Si  0.0000  0.1196(3)  0.6175(4)  1.000  8  h  ?  d  Biso  0.23(3)
O1  O   0.0000  0.2500  0.2148(9)  1.000  4  e  ?  d  Biso  0.23(3)
O2  O   0.0000  0.2500  0.7195(9)  1.000  4  e  ?  d  Biso  0.23(3)
O3  O   0.0000  0.9915(4)  0.2561(9)  1.000  8  h  ?  d  Biso  0.23(3)
O4  O   0.2631(5)  0.1226(14)  0.9942(4)  1.000  16 j  ?  d  Biso  0.23(3)

```

```

data_Wadsleyite
_audit_creation_method 'Created with CONVERT.DLL (www.crystalimpact.com)'
_audit_creation_date 2011-09-04
_audit_update_record 2011-09-04
_journal_codem_ASTM ?
_journal_year ?
_journal_volume ?
_journal_page_first ?
_journal_page_last ?
_publ_author_name '?,'
_publ_section_title
;
' 929'
;
_chemical_formula_sum 'Mg16 Si8 O32'
_chemical_formula_weight 1125.545
_cell_length_a 5.7321(1)
_cell_length_b 11.4998(2)
_cell_length_c 8.3163(2)
_cell_angle_alpha 90.000
_cell_angle_beta 90.000
_cell_angle_gamma 90.000
_cell_volume 548.2(0)
_symmetry_int_tables_number 74
_symmetry_space_group_name_H-M 'I m m a'
_symmetry_space_group_name_Hall '-I_2b_2'

loop_
_symmetry_equiv_pos_site_id
_symmetry_equiv_pos_as_xyz
1 x,y,z
2 -x,0.500-y,z
3 x,-y,-z
4 -x,0.500+y,-z
5 -x,-y,-z
6 x,0.500+y,-z
7 -x,y,z
8 x,0.500-y,z
9 0.500+x,0.500+y,0.500+z
10 0.500-x,1.000-y,0.500+z
11 0.500+x,0.500-y,0.500-z
12 0.500-x,1.000+y,0.500-z
13 0.500-x,0.500-y,0.500-z
14 0.500+x,1.000+y,0.500-z
15 0.500-x,0.500+y,0.500+z
16 0.500+x,1.000-y,0.500+z

loop_
_atom_type_symbol
_atom_type_oxidation_number
_atom_type_radius_bond
Mg ? 1.200
Si ? 1.200
O ? 1.200

```

```
loop_  
_atom_site_label  
_atom_site_type_symbol  
_atom_site_fract_x  
_atom_site_fract_y  
_atom_site_fract_z  
_atom_site_occupancy  
_atom_site_symmetry_multiplicity  
_atom_site_Wyckoff_symbol  
_atom_site_attached_hydrogens  
_atom_site_calc_flag  
_atom_site_thermal_displace_type  
_atom_site_u_iso_or_equiv  
Mg1 Mg  0.0000  0.0000  0.0000  1.000  4  a ? d Biso  0.41(4)  
Mg2 Mg  0.0000  0.2500  0.9697(5)  1.000  4  e ? d Biso  0.41(4)  
Mg3 Mg  0.2500  0.1301(5)  0.2500  1.000  8  g ? d Biso  0.41(4)  
Si1 Si  0.0000  0.1188(3)  0.6163(4)  1.000  8  h ? d Biso  0.41(4)  
O1 O  0.0000  0.2500  0.2164(10)  1.000  4  e ? d Biso  0.41(4)  
O2 O  0.0000  0.2500  0.7147(10)  1.000  4  e ? d Biso  0.41(4)  
O3 O  0.0000  0.9907(4)  0.2538(10)  1.000  8  h ? d Biso  0.41(4)  
O4 O  0.2639(6)  0.1235(13)  0.9939(5)  1.000  16 j ? d Biso  0.41(4)
```

```

data_Wadsleyite
_audit_creation_method 'Created with CONVERT.DLL (www.crystalimpact.com)'
_audit_creation_date 2011-09-04
_audit_update_record 2011-09-04
_journal_codem_ASTM ?
_journal_year ?
_journal_volume ?
_journal_page_first ?
_journal_page_last ?
_publ_author_name '?,'
_publ_section_title
;
' 1084'
;
_chemical_formula_sum 'Mg16 Si8 O32'
_chemical_formula_weight 1125.545
_cell_length_a 5.7391(1)
_cell_length_b 11.5134(2)
_cell_length_c 8.3350(2)
_cell_angle_alpha 90.000
_cell_angle_beta 90.000
_cell_angle_gamma 90.000
_cell_volume 550.7(0)
_symmetry_int_tables_number 74
_symmetry_space_group_name_H-M 'I m m a'
_symmetry_space_group_name_Hall '-I_2b_2'

loop_
_symmetry_equiv_pos_site_id
_symmetry_equiv_pos_as_xyz
1 x,y,z
2 -x,0.500-y,z
3 x,-y,-z
4 -x,0.500+y,-z
5 -x,-y,-z
6 x,0.500+y,-z
7 -x,y,z
8 x,0.500-y,z
9 0.500+x,0.500+y,0.500+z
10 0.500-x,1.000-y,0.500+z
11 0.500+x,0.500-y,0.500-z
12 0.500-x,1.000+y,0.500-z
13 0.500-x,0.500-y,0.500-z
14 0.500+x,1.000+y,0.500-z
15 0.500-x,0.500+y,0.500+z
16 0.500+x,1.000-y,0.500+z

loop_
_atom_type_symbol
_atom_type_oxidation_number
_atom_type_radius_bond
Mg ? 1.200
Si ? 1.200
O ? 1.200

```

```
loop_  
_atom_site_label  
_atom_site_type_symbol  
_atom_site_fract_x  
_atom_site_fract_y  
_atom_site_fract_z  
_atom_site_occupancy  
_atom_site_symmetry_multiplicity  
_atom_site_Wyckoff_symbol  
_atom_site_attached_hydrogens  
_atom_site_calc_flag  
_atom_site_thermal_displace_type  
_atom_site_u_iso_or_equiv  
Mg1 Mg  0.0000  0.0000  0.0000  1.000 4 a ? d Biso  0.39(4)  
Mg2 Mg  0.0000  0.2500  0.9670(5)  1.000 4 e ? d Biso  0.39(4)  
Mg3 Mg  0.2500  0.1286(5)  0.2500  1.000 8 g ? d Biso  0.39(4)  
Si1 Si  0.0000  0.1203(4)  0.6168(4)  1.000 8 h ? d Biso  0.39(4)  
O1 O  0.0000  0.2500  0.2152(9)  1.000 4 e ? d Biso  0.39(4)  
O2 O  0.0000  0.2500  0.7154(10)  1.000 4 e ? d Biso  0.39(4)  
O3 O  0.0000  0.9912(4)  0.2551(10)  1.000 8 h ? d Biso  0.39(4)  
O4 O  0.2657(6)  0.1255(15)  0.9939(5)  1.000 16 j ? d Biso  0.39(4)
```